FISEVIER

Contents lists available at ScienceDirect

Thin-Walled Structures

journal homepage: www.elsevier.com/locate/tws



Full length article

Response characterization of multistable shallow domes with cosine-curved profile



Mansour Alturki^a, Rigoberto Burgueño^{b,*}

- ^a Department of Civil and Environmental Engineering, 3504 Engineering Building, Michigan State University, East Lansing, MI, 48824-1208, USA
- b Department of Civil and Environmental Engineering, Department of Mechanical Engineering, 3574 Engineering Building, Michigan State University, East Lansing, MI, 48824-1226, USA

ARTICLE INFO

Keywords: Shells Buckling Instability Snap-through Post-buckling

ABSTRACT

The multistable elastic behavior of a shallow dome with a cosine-curved profile is investigated in this work. The dome exhibits snap-through instability and could be used as a building block for energy dissipation mechanism in structures subjected to cyclic loading and high deformation demands. Numerical and experimental studies were carried on the geometric and material properties of the cosine-curved domes (CCD) under concentrated load at the apex. Finite element analyses (FEA), validated by experimental tests on 3D printed specimens, were conducted to study the controlling geometric and material properties of the CCD. Three types of response were recognized and discussed based on the force- and strain energy-displacement curves. Limitations on the geometric parameters that govern the recoverability of the original shape and the stability state upon load removal are also identified. In addition, empirical relations to estimate the limit-point load and displacement, and to characterize the snap-through response were developed. Good agreement was observed using the determined limits on the geometric parameters and the developed relations with the results from FEA and experimental tests.

1. Introduction

A new shallow dome-shaped structural element that exhibits multistable elastic behavior is presented in this paper. The element offers reliable and reversible large elastic deformation that could be used as a building unit for devices subjected to relatively high forces [1] for energy dissipation and repeated use. Such devices usually have a hysteretic response that is based on consecutive snap-through instabilities of a sufficient number of units that are connected in series [2].

The interest in studying shallow domes originates from the fact that they can be fabricated in curved revolved profiles (i.e., aside from spherical shapes) that allow them to have a tunable multistable response. These domes can snap-through to a new configuration within their elastic range of response and snap-back with or without a restoring external force without damage. This deformability enables these domes to absorb and/or trap strain energy (*U*) and release all or a part of it to restore their original configuration [3].

Several multistable elements with the ability to exhibit snapthrough instability with large elastic (reversible) deformations have been investigated and reported. Such elements can be used as the building units in many structures utilized to elastically absorb and dissipate energy [4–9]. Most of these structures are based on two basic types of multistable elements: (a) inclined beams or bars [5], and (b) curved beams or bars [10]. Although these structures show the ability to absorb shocks and dissipate energy, they possess some design disadvantages when considering large-scale applications where high force levels are expected, such as applications for seismic protection in buildings and bridges. These disadvantages include high stress concentrations at the elements' constraining edges, low relative threshold forces, and the requirement of constraining other buckling modes to attain a symmetric deformation response.

Many other structures have been investigated to obtain multiple elastic instabilities for a multistable response. The simplest is an elastic compressed column with continuous bilateral constraints [11,12]. In such a system, compressive axial load is applied to the column causing it to buckle multiple times in an elastic post-buckling regime before reaching material damage. Another example are tilted beams under vertical loading [5,6], where a constrained tilted beam snaps-through to a new stable configuration. Single and double curved beams loaded at their apex [10,13] are also capable of attaining snap-through instability. Another example are tailored cylindrical shells under axial compressive loading [14,15], where geometric imperfections are seeded into specific regions to control the elastic post-buckling response. Shallow arches and lattice domes are also capable of attaining

E-mail addresses: alturki1@msu.edu (M. Alturki), burgueno@msu.edu (R. Burgueño).

^{*} Corresponding author.

multistable elastic responses through snap-through instabilities or snap-through buckling [16–19]. The common phenomenon among these structures is that they undergo elastic post-buckling response after reaching a critical point. However, they differ in their post-buckling behavior and their relative deformability.

The stability, buckling capacity, post-buckling behavior, and deformation symmetry of spherical domes under a concentrated load at the apex have been the subject of several studies. Mescall [20] performed a numerical study by solving the nonlinear equations governing the axisymmetric deformations of spherical shells, for unrestrained and clamped edges, to examine the effects of geometric parameters and boundary conditions on their response. Penning [21] conducted an experimental investigation to study buckling deformations of clamped spherical shells under a concentrated load. Fitch [22], and Brodland and Cohen [23] conducted an analytical study to investigate the deflection, snap-through buckling, and the occurrence of asymmetric bifurcation points before axisymmetric snap-buckling, by examining a single parameter (λ) that governs this phenomenon for clamped and unrestrained shallow spherical domes. This geometry parameter depends on the geometric and material properties of the domes and is given by Eq. (1), where a and b are the spherical and base radii, respectively, t is the uniform thickness, and ν is the Poisson ratio. It was concluded that asymmetric bifurcation occurs when a spherical dome becomes deeper and thinner (i.e., higher values of λ).

$$\lambda = [12(1-\nu^2)]^{1/4}b/(a\ t)^{1/2}.\tag{1}$$

Brinkmeyer et al. [24] and Madhukar et al. [25] also performed combined experimental and numerical studies using finite element analyses (FEA) to examine the effects of geometric and material properties on the stability state of unrestrained spherical domes. Brinkmeyer et al. [24] found that pseudo-bistability occurs for domes when $5.31 \le \lambda \le 5.35$. Madhukar et al. [25] proposed an expression for pseudo-bistability that depends on the geometric parameters of a dome.

The study conducted by Mescall [20] showed that spherical domes with unrestrained and clamped edges could display snap-through instability. Unrestrained domes required $\lambda > 3.75$ to display snap-through, while clamped domes required $\lambda \geq 9$. However, the study by Fitch [22] showed that spherical domes with clamped edges and $\lambda \geq 9.2$ would have a bifurcation point and asymmetric deformations at a load below the critical load for axisymmetric snapping instability. These two findings impose a very narrow range of λ (i.e., 9 to 9.2) for spherical domes with clamped edges to display axisymmetric snapthrough response. Therefore, it seems that clamped spherical domes cannot practically have reversible axisymmetric snap-through instability even when the previous two limits are met. In contrast, this investigation shows that the shallow cosine-curved domes (CCD) proposed here have a wide range of geometric ratios for which symmetric snap-through is achievable.

The interest in domes with clamped edges originates from that fact that they can be used in many structural applications as an integrated part of systems, compared to domes with unrestrained edges. For example, the shock absorbers proposed in Refs. [4–7] consist of multistable elements as unit cells where each unit is attached to the adjacent units via rigid segments that provide system integrity to resist a common load, as well as the required constraints for individual units to respond in the desired way.

In this work, numerical and experimental studies were carried out to study the effects of the geometric and material properties on the behavior of multistable CCDs under a concentrated transverse load, and to characterize the resulting force-deformation response. This is accomplished by conducting a parametric study using experimentally validated FEA on the properties governing the response of the CCD. The limit that governs the transitional state between bistable and monostable states is identified, and a simple expression is proposed to facilitate the design of CCDs with a desired stability state. Empirical design expressions were developed for the controlling parameters to

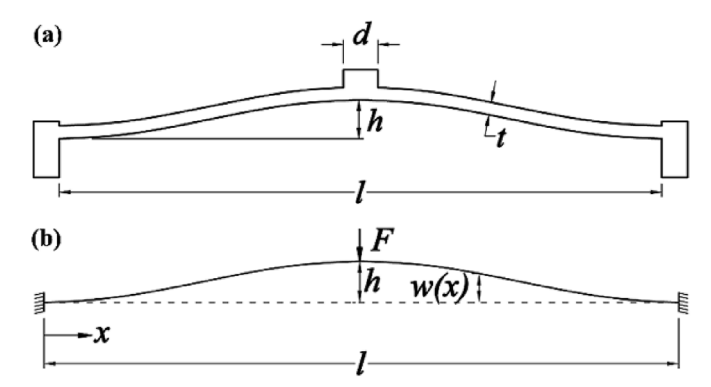


Fig. 1. Geometric parameters of a typical CCD: (a) a cross-section at the apex, and (b) the idealized system.

construct a simplified multilinear response that could be used to calculate the response for a system of multiple CCDs, which can attain controllable energy dissipation characteristics.

2. Methods

2.1. Research aim and scope

The cross-sectional profile shape of the proposed CCD is based on the cosine function given in Eq. (2) [26], where w(x) is the vertical distance from the horizontal chord line to the dome's profile shape at a distance x from the circumference as shown in Fig. 1. The dome's base along its circumference is connected to a rigid ring that constrains rotations and edge sliding of the dome under loading.

$$w(x) = h/2[1-\cos(2\pi x/l)]$$
 (2)

This equation represents the shape of the first buckling mode of a fixed-fixed straight beam under axial compressive loading. The benefit of using the cosine-curved shape over a spherical one is that it enables the dome to have a symmetric snap-through to a monostable or a bistable state. This profile was inspired by the shape of curved double beams loaded laterally [10]. However, unlike the curved double beams, a CCD doesn't require restricting other buckling modes to have a symmetric reversible snap-through response. They also have lower stress concentrations at the supporting edge compared to systems composed of curved double beams or inclined beams.

The scope of this study is thus on the response of shallow CCDs that, upon being transversely loaded at their apex, display an elastic response and limit-point critical instability with a snap-through geometrical transition. When a shallow CCD is loaded beyond its limit-point it snaps-through to a new configuration. The force-deformation response is nonlinear before and after the limit-point snap-through instability (initial loading path and unstable path), with a fairly linear response upon continued loading in the new configuration (Fig. 2). While the unstable response path (negative tangent stiffness) cannot be obtained under force-controlled loading, it can be attained in a stable manner under displacement-controlled loading. Snap-through instability, also called limit-point instability or snap instability, does not involve any bifurcation of the equilibrium path [3].

The stability of the new configuration depends on the dome's geometric and material properties [3]. The response of a CCD under loading force (F) can be classified into three categories as shown in Fig. 2 [25]. Each type of response depends mainly on the shape of the strain energy-displacement (U- δ) curve and is related to the force-displacement curve (F- δ) [25].

Fig. 2(a) and (d) show a bistable response, where the U- δ curve has a local maximum strain energy point, $U_{\rm max}$, and a local minimum strain energy point, $U_{\rm min}$, at non-zero displacements before the energy (U) continues to increase with increasing displacement (δ). In this response,

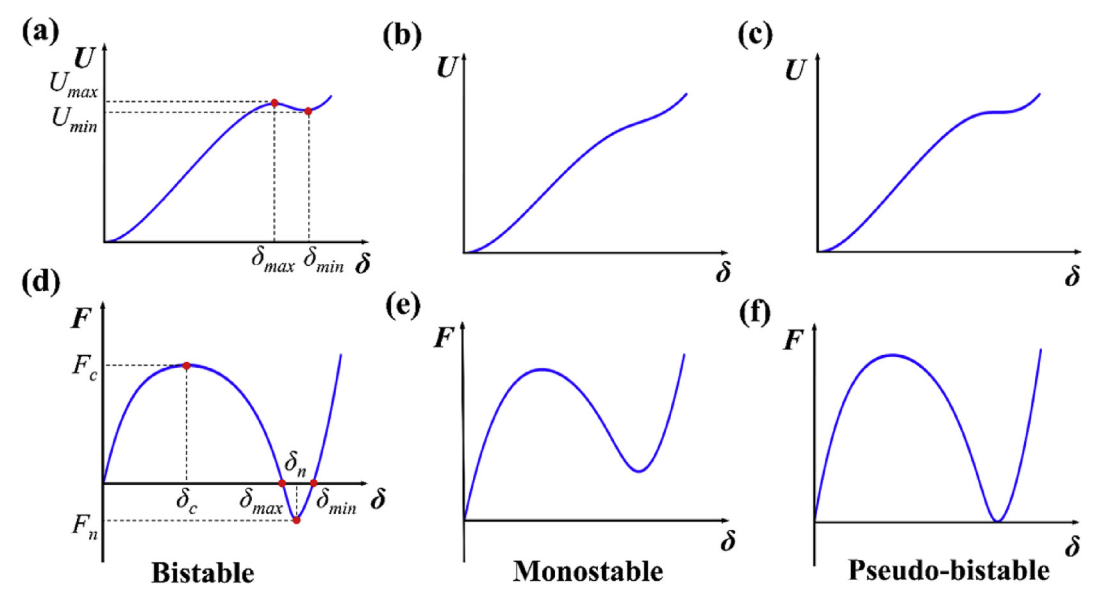


Fig. 2. Typical strain energy-displacement and force-displacement responses of CCDs.

a CCD snaps into a new configuration and cannot restore its original configuration upon unloading without the application of an external restoring force (i.e., not self-recoverable). In this case, some of the induced energy is trapped in the system and hence the F- δ curve has a negative force (in opposite direction to the deformation being generated) part.

A monostable response (Fig. 2(b) and (e)) is defined when the E- δ curve is monotonic and the F- δ curve has no negative force part. In this type of response, a CCD snaps back to its original configuration upon unloading, without application of an external restoring force, as long as material damage does not occur.

In a pseudo-bistable response (Fig. 2 (c) and (f)) the $E-\delta$ curve has a flat segment (i.e., $U_{\rm max}=U_{\rm min}$) before the energy continues to increase with increasing δ , and the $F-\delta$ curve has a zero force value at a non-zero displacement. This response represents a transition state between bistable and monostable responses where a CCD snaps and restores its original configuration after unloading, and without the application of an external restoring force, but with a delay depending on the viscoelastic properties of the material [24].

2.2. Modeling and analysis

The CCD element studied was idealized as shown in Fig. 1(b). The dome's horizontal orientation is along the shown x-axis and the vertical direction is perpendicular to it. The dome is modeled with clamped boundary conditions along its base circumference. Loading is assumed to be applied by a vertical concentrated load (F) at the dome's apex, and directed downwards. The applied load causes a vertical (transverse) displacement δ . The key geometric parameters on the CCD's response are the uniform thickness, t, the base diameter or span length, l, the apex height, h, and the diameter of the loading area, d, as shown in Fig. 1 (a). The CCDs examined here are considered shallow and thin shells with a height-to-span ratio of less than 1/5 and a thickness-to-radius of curvature ratio of less than 1/20 [1].

Nonlinear geometric finite element analyses (FEA) were used to examine the force-deformation responses of CCDs using the program ABAQUS [27]. The CCD was modeled as a 3D deformable revolved shell object with linear elastic isotropic material properties and four-node shell elements (S4) for the mesh. The mesh size was selected based on a mesh refinement study. Displacement control was used to apply a static incremental displacement at the dome's apex, and large deformations were accounted for by considering geometric non-linearity in the

analyses. Eigenvalue analyses were conducted to verify predicted snapthrough instability by confirming that the bifurcation loads were higher than the limit-point load. For cases where the analyzed CCD was deep and thin (i.e., high h/t), the automatic stabilization option in ABAQUS's solver was used to facilitate a converged solution.

2.3. Experimental validation

Experimental tests were conducted on 3D printed CCDs to examine the three stability states presented in Fig. 2, and to compare the experimentally obtained F- δ response to those generated from the FEA. The CCDs were fabricated using a 3D polymer-based printer (MakerBot Replicator 2) with polylactic acid (PLA) filament. Due to imperfections from the manufacturing process the "as printed" dimensions varied slightly (about 10%) from the nominal design values. The design and the "as-printed" dimensions for the test specimens are given in Table 1. This is important since small changes in t or h significantly change the dome's response and the desired stability state. Thus, the FEA simulations were based on the 'as-printed' dimensions. The PLA material has a reported Poisson's ratio, ν , of 0.33 and an average modulus of elasticity, E, of 1582 MPa [4].

Tests were performed using a universal testing machine with custom

 Table 1

 Design and 'as-printed' dimensions of experimentally tested CCDs.

Specimen	Design dimensions			'As-printed' dimensions		
	t (mm)	h (mm)	l (mm)	t (mm)	h (mm)	l (mm)
1M	1.5	5.00	120.0	1.82	4.58	119.3
2M	1.5	5.00	120.0	1.74	4.46	119.2
3B	1.00	6.00	100.0	1.26	5.66	98.4
4B	1.00	6.00	100.0	1.17	5.67	98.7
5M	0.84	3.20	102.0	1.13	2.78	100.4
6M	1.00	3.20	102.0	1.18	2.91	101.7
8P	1.20	5.00	100.0	1.39	4.41	101.5
8P	1.20	5.00	128.8	1.45	4.29	126.9
9B	0.60	3.50	60.0	0.70	3.40	59.9
10B	0.60	3.50	60.0	0.87	2.91	59.8
11P	0.60	2.00	50.0	0.72	1.97	49.9
12B	0.60	2.60	60.0	0.74	2.62	59.9
13M	0.65	2.50	65.0	0.86	2.50	64.9
14M	0.60	1.80	50.0	0.73	1.76	50.9

Note: M: monostable, B: bistable, P: pseudo-bistable.

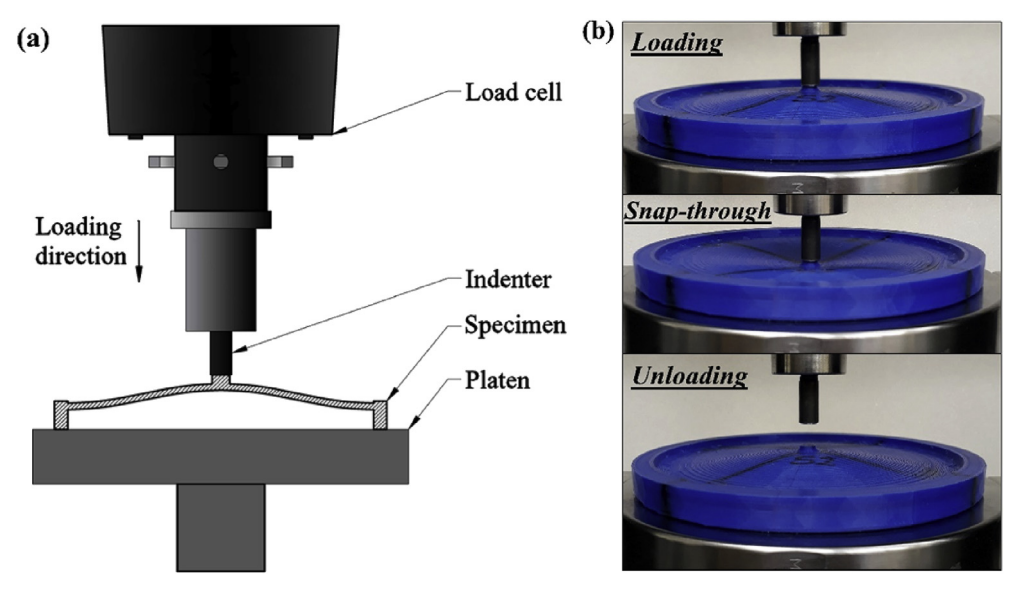


Fig. 3. (a) Test setup for CCD under axial compression; and (b) loading stages for a monostable CCD.

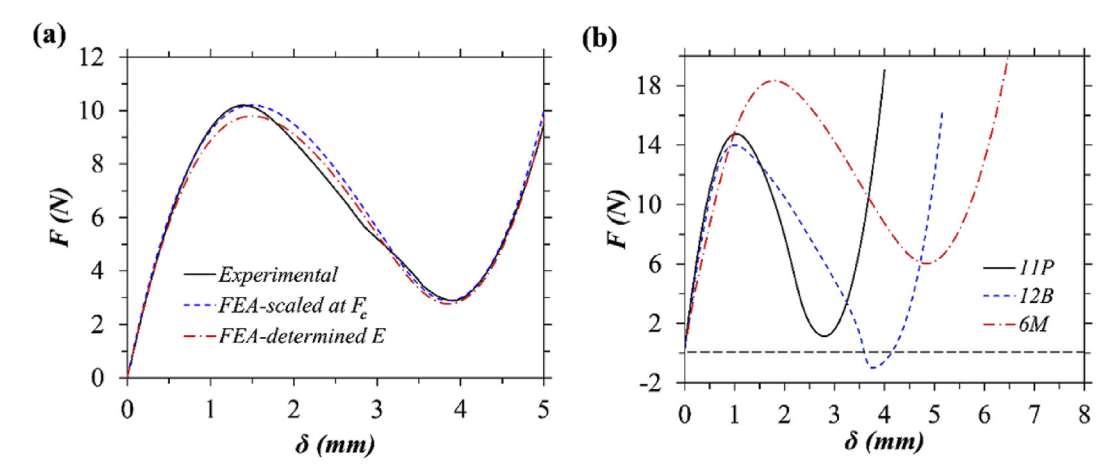


Fig. 4. (a) F- δ curves for specimen 5M from experiment compared to FEA, and (b) experimental F- δ curves for specimens 11P, 12B, and 6M.

fixtures (indenter) to apply a concentrated vertical load at the CCD apex, as shown in Fig. 3. Loading was done under displacement control, applying an incremental displacement at a constant rate of 0.1 mm/s. For CCD specimens with bistable response ($F_n < 0$), the loading indenter was mechanically attached to the apex of the CCD and the specimen was also clamped to the platen. Fig. 4 shows experimental F- δ responses for CCD specimens with 'as-printed' dimensions as given in Table 1.

The actual modulus of elasticity of a 3D printed part is highly sensitive to the orientation of the printed layers and to the direction of loading [28,29]. For example, the investigation conducted by Perkowski [30] on the mechanical properties of 3D printed PLA parts showed that the modulus of elasticity ranged from about 550 to 3100 MPa in tension and from 570 to 1650 MPa in compression. Therefore, the FEA F- δ response in Fig. 4 was scaled for E so that F_b was equal to that of the experimentally measured data. The scaling factor was determined by conducting a FEA for a CCD with 'as-printed' dimensions and an elastic modulus value of unity and then dividing the value of F_c (or any other value) on the experimental $F-\delta$ curve by its counterpart of the same displacement on the FEA curve. The scaling factor was 851 MPa, which represents the most representative value of E for the specimen. This procedure is valid as long as most parts of the two curves coincide; however, an exact agreement cannot be obtained because of the presence of imperfections and the non-uniformity of the

'as-printed' dimensions. Moreover, this procedure is only valid for elastic responses as discussed in Section 4.5. Fig. 4(a) shows a comparison between the experimental and numerical (FEA) F- δ responses for CCD specimen 5M with 'as-printed' dimensions (given in Table 1). Fig. 4(a) shows two F- δ responses from FEA based on (1) the scaling factor and (2) an average value for E of 817 MPa. This value of E was determined from a series of tests on 3D printed ASTM D695 specimens, for which the print layers were oriented perpendicularly to the longitudinal axis to closely represent the loading conditions of the tested CCDs.

3. Parametric study

A parametric study was carried out on the geometric parameters t, l, h, and d (see Fig. 1), and the material properties E and ν , to study their effects on the response of CCDs. The study was conducted using FEA by systemically varying one of the parameters, while keeping the others unchanged. The investigated response quantities (see Fig. 2(d)) were the critical limit load, F_c , the critical displacement, δ_b , the negative or minimum force, F_n , and the non-zero displacement at the minimum force, δ_n . The study also evaluated the resulting shape of the F- δ curve since it characterizes the post-buckling behavior. Moreover, normalizing ratios such as δ/h and h/t were used to study the curve shapes. The study was conducted for CCDs with $1.5 \le h/t \le 7.5$ and $h/l \le 1/16$ [1].

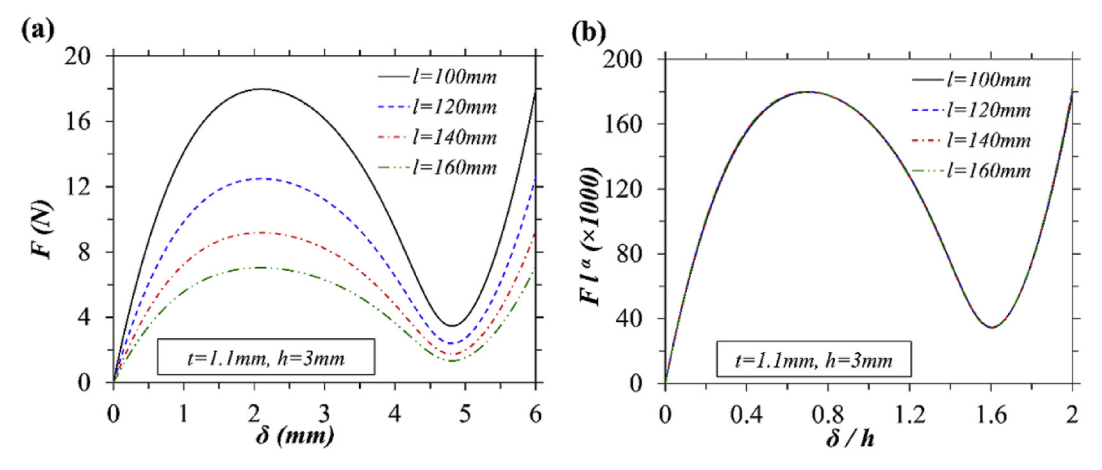


Fig. 5. Actual and normalized $F-\delta$ curves of CCDs with constant t and h, and varying l.

The FEA were performed by varying l and fixing t and h and then repeating the same process for different values of t and h. The material constants were kept unchanged at E=1500 MPa and $\nu=0.33$.

As discussed earlier, the F- δ curve is related to the U- δ curve (Fig. 2). The difference between the maximum and minimum strain energies, ΔU , (i.e., $\Delta U = U_{\rm max} - U_{\rm min}$) is directly related to the value and the mathematical sign of F_n , and hence the stability state of a CCD. When ΔU is greater than zero F_n is negative and the response is bistable. When ΔU equals to zero F_n also equals zero and the response is pseudo-bistable. Local maxima and minima do not exist when the U- δ curve is monotonic, hence F_n is greater than zero and the response is monostable. Therefore, this study focuses on the F- δ curve rather than the U- δ curve to examine the stability states since dealing with a single quantity (F_n) is easier than dealing with two quantities $(U_{\rm max}$ and $U_{\rm min})$.

3.1. Effect of length (l)

The effect of varying l on the F- δ response curve is shown in Fig. 5(a). The values of F_c and $|F_n|$ decrease with an increase in l, while $\delta_{\rm C}$ and $\delta_{\it n}$, are not affected by the change in *l*. To further examine the effect of varying l on the shape of the $F-\delta$ curves it is necessary to normalize them to a factor in terms of l. A least square regression analysis [31] was used to determine the value of a power " α " for a factor l^{α} to be multiplied by F for constant values of t and h. Since the curves may have different post-buckling responses, regression analyses were performed on the values of F_c , which resulted in $\alpha = 2$. It was found that normalizing the $F-\delta$ curves by the factor l^2 results in exact agreement among them over the entire response range (pre- and postbuckling) as shown in Fig. 5(b). This shows that l has no effect on the type of response of the CCD. Thus, for example, if the F- δ response has a bistable shape, then this response type will not change to a monostable or pseudo-bistable by changing l. The reason is that since the examined CCDs are shallow where the span-length l is much larger than the thickness t and the apex height h, the variation in length has an insignificant effect on the ratios h/l and t/l.

3.2. Effect of thickness (t)

A similar procedure was followed by analyzing CCDs with varying t while fixing other parameters. Analysis results show that t has a dominant effect on the shape of the F- δ response curve, as shown in Fig. 6(a), where the values of F_c and F_n can be seen to increase with an increase in t. In addition, by increasing t the response changed from bistable to monostable. This means that F_n increases relative to F_c and that the ratio h/t is decreasing.

The force values in the curves of Fig. 6(a) need to be normalized in terms of t to compare them and assess the effect of t. A least squares

regression analysis [31] was used to determine the value of " β " for the factor 1/t $^{\beta}$ for constant values of h. For this case the value of l has no effect on β , and hence it was not included in the analysis. Since the curves have different post-buckling responses, the regression analysis was performed only on the values of F_b to find β . A constant value of $\beta = 2.412$ was found. The same value of β would be determined if the regression analysis was performed on the F- δ curve data up to F_c .

The normalized curves are shown in Fig. 6(b). Comparing Fig. 6(a) and (b) shows that $\delta_{\rm C}$ and $\delta_{\rm C}/h$ are roughly the same for all cases and thus they are only slightly affected by the change in t or h/t. On the other hand, δ_n and δ_n/h decrease with increasing t or decreasing h/t. From Fig. 6(b), the normalized values of F_c are approximately the same for varying t, while they are different for the case of F_n because of the change in post-buckling behavior.

3.3. Effect of height (h)

Analysis results showed that CCD height (h) has a complex effect on the shape of the F- δ curves, as shown in Fig. 7(a). This effect can be grouped into three features: (1) F_c increases with h, similar to the effect of t; (2) F_n decreases with h, opposite to the effect of t; and (3) h increase shifts the F- δ curve with increased values for the critical displacements δ_C and δ_n . It can be construed that the ratio h/t mainly controls the shape of the F- δ curve and hence the stability state. Fig. 7(a) also shows that δ_C and δ_n , increase with an increase in h or h/t.

The force values in Fig. 7(a) were normalized with the factor $1/h^{\gamma}$ in order to examine the shape of the F- δ curves. The normalized curves are shown in Fig. 7(b). The value of " γ " was determined to be equal to 1.582 through a least squares regression analysis on the values of F_c . The normalized curves in Fig. 7(b) show that δ_C/h is approximately the same for all cases and thus they are only slightly affected by the change in h. On the other hand, δ_n and δ_n/h increase with increasing h. The normalized values of F_c are roughly the same with varying h while they are different for the case of F_n because of the change in post-buckling behavior.

3.4. Effect of loading area

Another important parameter that affects the shape and the values of the F- δ curves is the loading area, that is, the circular region around the apex point where the dome is loaded, see Fig. 8. Since in most applications a theoretical point load cannot be practically applied, there is a finite area over which the load is distributed. In this study the area is assumed to be circular and perpendicular to the axis of rotation of a CCD. It was found that the size of this area has a significant effect on the shape of the F- δ curve, but a minimal effect on the stability state a CCD. Fig. 8(a) shows the effect of increasing the diameter of the loading area

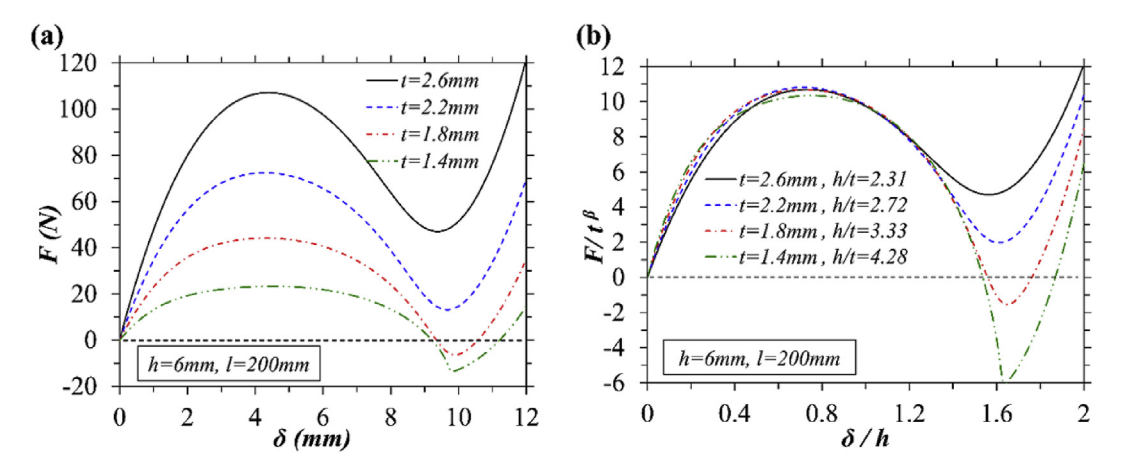


Fig. 6. Actual and normalized $F-\delta$ curves of CCDs with constant h and l, and varying t.

(d) on the F- δ curves for monostable and bistable CCDs. It is shown that the values of F_c increase with an increase in d; while the values of F_n slightly increase for monostable responses and slightly decrease for bistable responses with an increase in d. In addition, the effect of d on the F- δ curve is more pronounced for deeper CCDs (i.e., CCDs with higher h/t). Increasing d also shifts the F- δ curve by decreasing the values of δ_C and δ_n .

If the loading area around the axis of rotation increases the original CCD area, as shown in Fig. 8(c), the loading area has a negligible effect on the response and hence the CCD should be treated as if d=0 with original length l. In other words, the loading area has no effect on the response as long as the loading region doesn't occupy an area of the original CCD's shape. The total span length (base diameter) is, however, increased by d (i.e., total span length is l+d). Nonetheless, this increase in length should not be considered in the analysis of the dome.

3.5. Effect of modulus of elasticity (E)

Since the concern here is the response of the CCD within the elastic range and for linear elastic material, the F- δ curve has a linear relationship with E and hence can be normalized by 1/E. To show that, several CCDs were analyzed for varying E, with all other parameters fixed and the resulting F- δ responses are shown in Fig. 9(a). It can be seen that F_c and $|F_n|$ increase with an increase in E. Fig. 9(a) also shows that δ_C and δ_n are the same for all cases, and thus unaffected by E. As expected, the F- δ curves for varying E collapse into each other when normalized by 1/E, see Fig. 9(b). Therefore, E has no effect on the shape of the E-E0 curves and the stability state of CCD if the material is linear elastic. The E-E1 curves can thus be scaled for different E2 values.

3.6. Effect of Poisson's ratio (ν)

Fig. 10 shows that F_c increases and F_n decreases with an increase in ν . It can also be observed that $\delta_{\rm C}$ and δ_n do not change for all cases, and thus they are not affected by ν . The shape of the F- δ curves is slightly affected by ν . As ν increases the response changes from monostable to bistable (and vice versa). Further, can be noted that F_n can become negative with increasing ν as shown in Fig. 10.

4. Design expressions for CCDs

The F- δ response in Fig. 11(a) is the result of a dynamic FEA for 12 monostable CCDs connected in series. Loading on the system was applied by displacement-controlled incremental deformation with geometric non-linearity considered in the analysis. The CCDs in the system were linked in series by connecting them at their confining rings and at the apex tips as shown in Fig. 11(b). The enclosed area between the loading and unloading curves represents the dissipated energy by the system. Studies by Benichou and Givli [32], and Restrepo et al. [33] showed that the response of a system of multistable units (e.g., Fig. 11(a)) can be accurately calculated based on the simplified multilinear response of a single unit, as that shown in Fig. 12. The approach greatly simplifies the analysis procedure and it is particularly convenient for design purposes. It is thus of interest to develop a simplified multilinear F- δ response curve for the CCD units.

Previous sections presented the studies of the effects of geometric and material properties on the F- δ response of CCDs, and a normalizing factor was determined for each parameter. These factors are now used to develop expressions for the key features of a CCD's F- δ response to

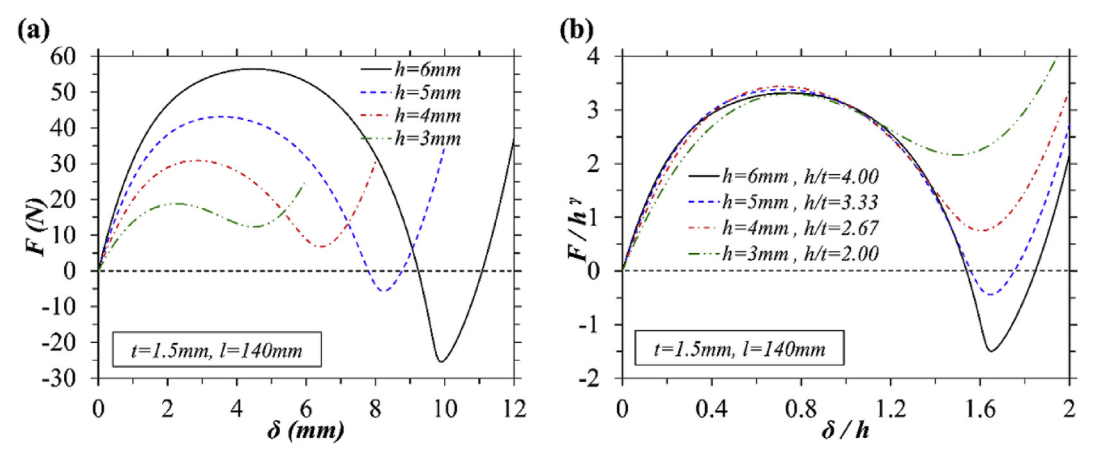


Fig. 7. Actual and normalized $F-\delta$ curves of CCDs with constant t and l, and varying h.

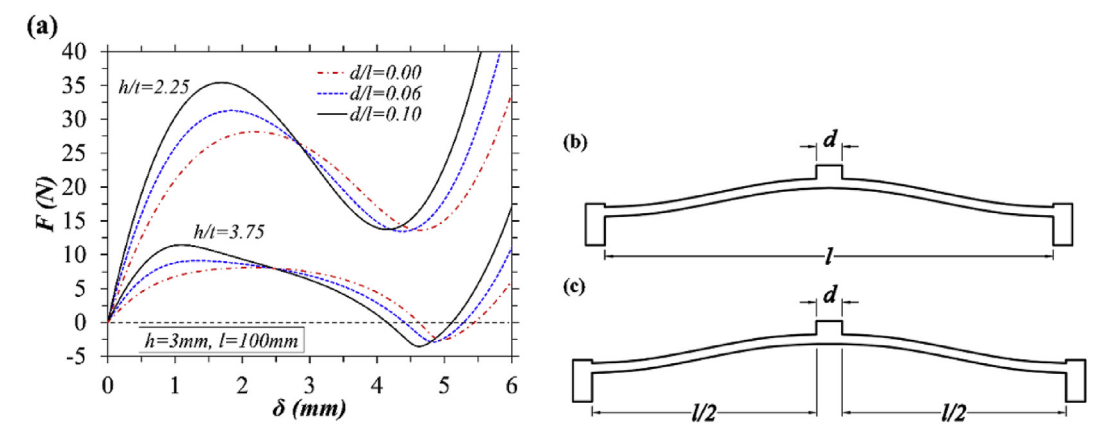


Fig. 8. (a) F- δ curves of CCDs with constant h and l, and varying h/t and d/l; (b) original profile shape of the CCD; and (c) modified shape of CCD with added loading area.

facilitate the construction of a multilinear response as shown in Fig. 12. It is recommended to use these expressions for CCDs with $1.5 \le h/t \le 4.5$ and $h/l \le 1/20$ for more accurate results. The objective is to use this simplified response to obtain the response for a system of multiple CCDs as shown in Fig. 11(a).

The multilinear response of a CCD (Fig. 12) is divided into three regions [33]: the initial stable equilibrium path in region I before the snap-through limit-point with an effective stiffness k_I , the unstable equilibrium, or snap-through, path in region II with negative stiffness k_{II} , and the post snap-through (or post-critical) stable path in region III with stiffness k_{III} . Defining the linear segments requires estimating the buckling load and displacement (F_b and δ_b), the minimum force and displacement (F_n and δ_n), and the post snap-through buckling stiffness (k_{III}).

In addition, it is of interest to know what type of stability would occur, that is, whether the CCD remains buckled (bistable) or restores to its original configuration (monostable) upon load removal. This can be achieved by knowing the conditions at which the pseudo-bistable response occurs. Thus, a study was also conducted to determine the governing factors of this stability state.

4.1. Critical limit-point (snap-through) load (Fc)

The value of F_c can be estimated by multiplying the inverses of the normalizing factors determined earlier by each other, in addition to a calibration factor, C_c , as given by Eq. (3).

$$F_c = C_c t^{\beta} h^{\gamma} E / l^{\alpha}. \tag{3}$$

The factor C_c is in terms of h/t and ν and can be calculated from the

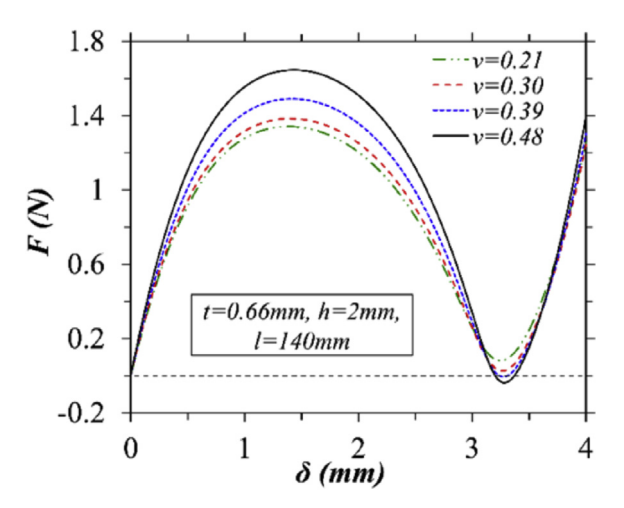


Fig. 10. F- δ curves of CCD with constant t, h, and l, and varying ν

FEA results by normalizing F_c by l^α/t^β h^γ E. Fig. 13 shows the calculated C_c values for h/t and ν . Each solid-line curve in Fig. 13 was approximated by a second-degree polynomial in terms of h/t and ν , as given in Eq. (4) with an absolute maximum error of about 2%.

$$C_c = (-0.466\nu - 0.251)(h/t)^2 + (3.304\nu^{0.27})(h/t) + (19.56\nu^{0.35})$$
 (4)

The value of C_c ranges from about 15 to 19 and can be simplified to a constant value of 17 with an 11.7% maximum absolute error.

As can be seen in Fig. 8(a), d has a significant effect on the F- δ

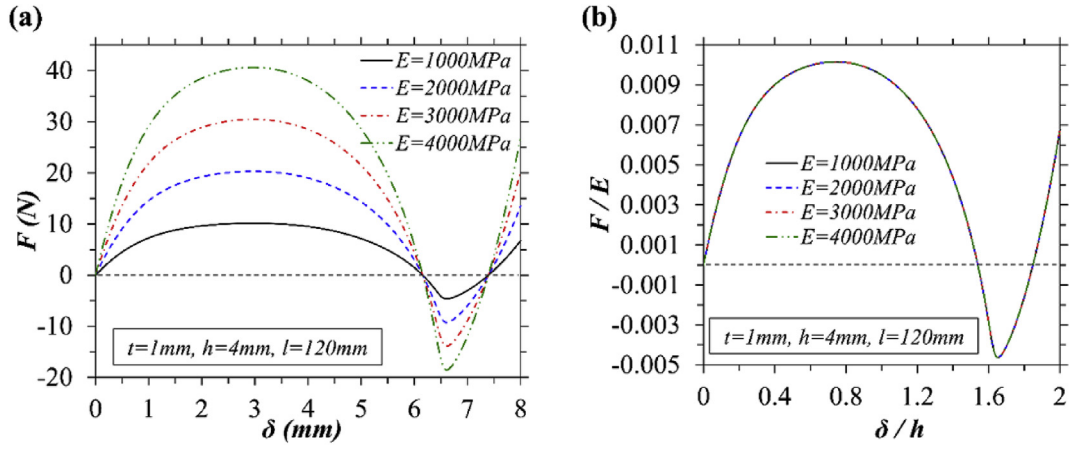


Fig. 9. Actual and normalized $F-\delta$ curves of CCDs with constant t, h and l, and varying E.

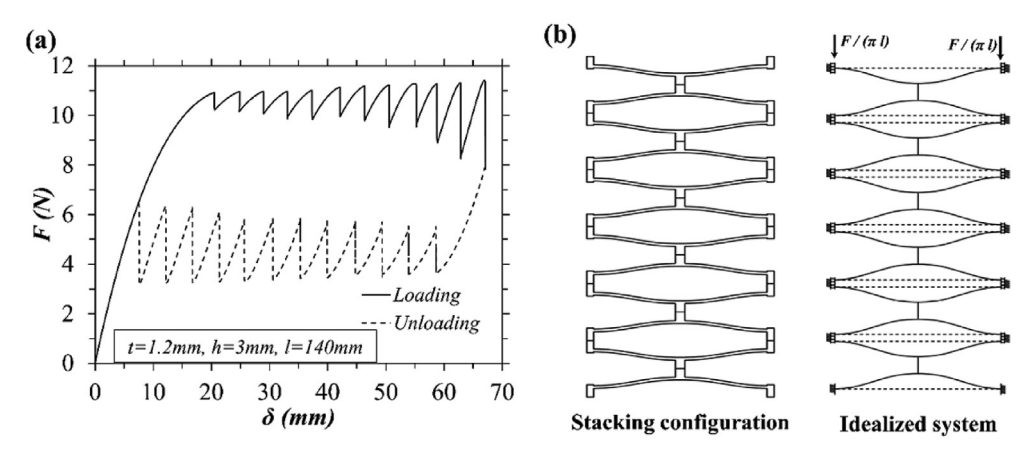


Fig. 11. Twelve monostable CCD units connected in series (a) hysteretic response from FEA, and (b) stacking configuration and idealized system.

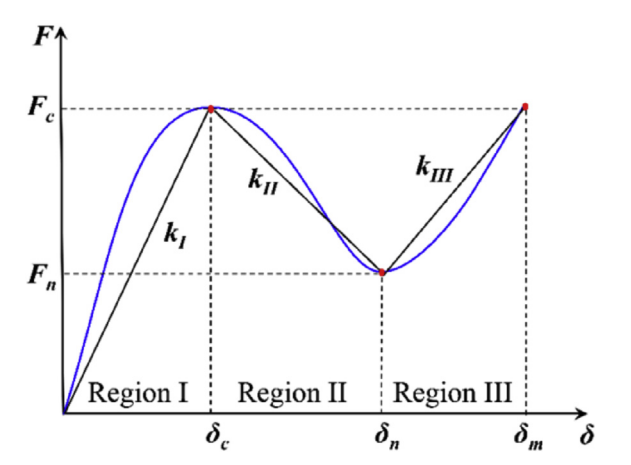


Fig. 12. Actual and multilinear F- δ responses of a CCD.

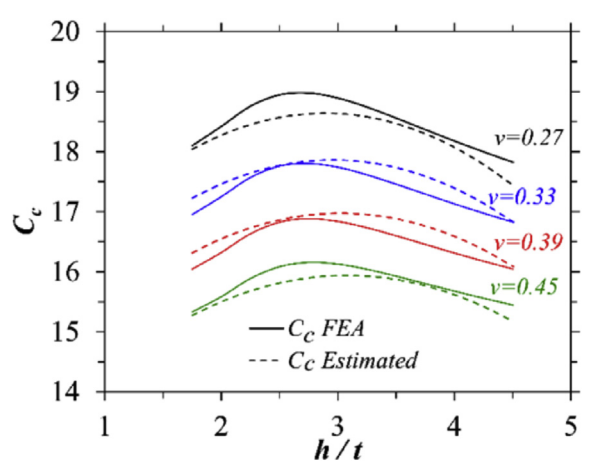


Fig. 13. C_c curves with h/t for different values of ν

response of CCDs, which in turn depends on h/t. To account for this effect, F_c and F_n values from FEA for CCDs with d>0 were normalized by the values of F_c and F_n with d=0. A relation was then established to determine a force modification factor, D, that is related to d/l and h/t as given in Eq. (5). Therefore, for CCDs with d>0 (as shown in Fig. 8(b) only), the buckling force F_c using Eq. (3) should be multiplied by D given in Eq. (5). This factor ranges from 1 to 1.43 and the expression is valid for $d/l \leq 0.1$.

$$D = 10.6(h/t)(d/l)^2 - 0.225(d/l) + 1 \ge 1$$
(5)

4.2. Minimum load (F_n)

An expression similar to Eq. (3) was used to estimate F_n with C_c replaced by C_n as given in Eq. (6). The factor C_n was also calculated by normalizing F_n from the FEA results by l^α/t^β h^γ E. Fig. 14 shows the calculated C_n values with h/t and ν . As can be seen, C_n changes sign from positive to negative with increasing h/t. Thus, this quantity controls the stability state at which the response of a CCD would be monostable or bistable. Fig. 14 also shows how the FEA results (solid-line curves) can be approximated by a second-degree polynomial in terms of h/t and ν , as given in Eq. (7). The value of F_n should also be modified by the force correction factor D given in Eq. (5) for CCDs with d>0.

$$F_n = C_n t^{\beta} h^{\gamma} E / l^{\alpha} \tag{6}$$

$$C_n = (0.336\nu + 0.889)(h/t)^2 - (13.06\nu + 10.82)(h/t) + (51.38\nu^{0.295}) \ge -12$$
(7)

4.3. Critical limit-point displacement (δ_c)

The value of $\delta_{\rm C}$ is related to h and is affected by h/t. Thus, it is best expressed as a ratio of h and in terms of h/t. Fig. 15 shows the calculated $\delta_{\rm C}/h$ against h/t from FEA results for several CCDs. The data points show that the relation between $\delta_{\rm C}/h$ and h/t is nonlinear and it was approximated by a second-degree polynomial. The following expression was developed for $\delta_{\rm C}/h$:

$$\delta_c/h = 0.061(h/t)^2 - 0.4(h/t) + 1.35 \tag{8}$$

For h/t > 4.5, Eq. (8) should be evaluated based on h/t = 4.5. Results from FEA compared to estimated values of $\delta_{\rm C}/h$ using Eq. (8) have average absolute error of less than 3%.

For CCDs with d>0 (as shown in Fig. 8(b) only), the calculated displacement $\delta_{\rm C}$ using Eq. (8) should be multiplied by a displacement correction factor, $G_{\rm c}$, that depends on d/l and h/t as given by Eq. (9). This factor should range from 0.42 to 1.

$$G_{c} = [-1.67(h/t) + 1.1](d/l) + 1 \le 1$$
(9)

4.4. Displacement at F_n (δ_n)

As for $\delta_{\rm C}$, δ_n was normalized by h and expressed in terms of h/t, and the data can be approximated by Eq. (10), see also Fig. 15. However, the relation of δ_n with respect to h/t seems simpler than that of $\delta_{\rm C}/h$, as shown in Fig. 15. For h/t > 4.5, δ_n/h should be calculated based on h/t = 4.5. The values of δ_n/h using Eq. (10) have an average absolute error of less than 2% with FEA results.

$$\delta_n/h = -0.081(h/t)^2 + 0.575(h/t) + 0.641 \tag{10}$$

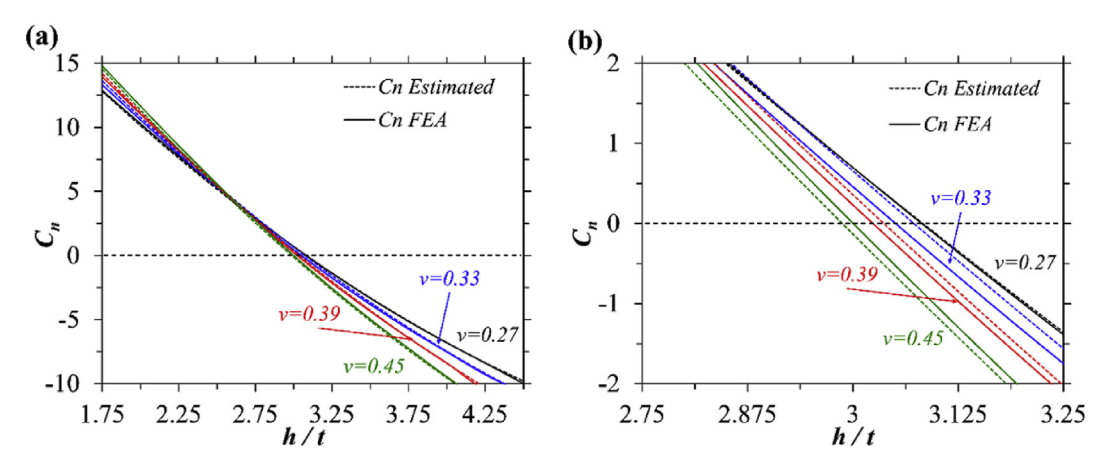


Fig. 14. (a) C_n curves with h/t for different values of ν , and (b) zoom-in at $C_n = 0$.

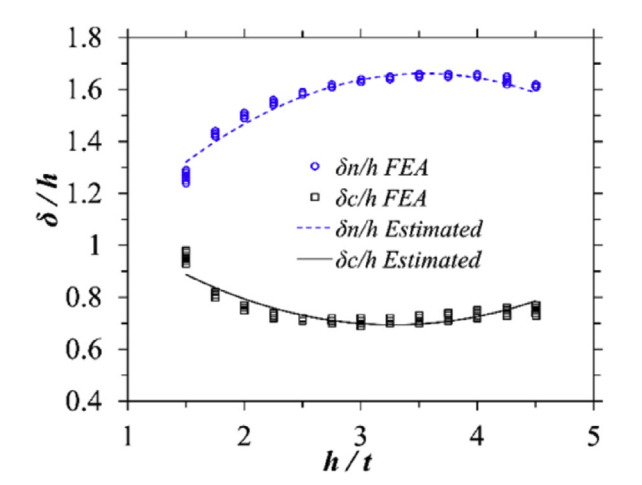


Fig. 15. Data and fit curves for $\delta_{\rm C}/h$ and δ_n/h with h/t.

For CCDs with d > 0, the displacement δ_n using Eq. (10) should be multiplied by a correction factor, G_n , that depends on d/l and h/t as given by Eq. (11). This factor should range from 0.89 to 1.

$$G_n = [0.24(h/t) - 1.43](d/l) + 1 \le 1$$
(11)

4.5. Post snap-through stiffness (k_{III})

At least two F- δ points are required to determine the stiffness k_{III} . The first point is the minimum force F_n at displacement δ_n . The second point is the limit-point force F_c at displacement δ_m , as shown in Fig. 12.

The displacement δ_m at F_c level was determined from FEA for various geometric and material properties. It was found that k_{III} can be expressed as a ratio of k_I . This ratio (k_{III}/k_I) is mainly affected by h/t and it ranges from 0 at about h/t = 1.45 to 2.78 for $h/t \ge 4.5$. As a result, Eq. (12) can be used to estimate k_{III}/k_I :

$$k_{III}/k_I = 0.9137(h/t) - 1.108 \le 2.78$$
 (12)

4.6. Limiting h/t for pseudo-bistable state

In Section 4 it was shown that only t, h, and ν affect the stability state of a CCD, and hence the shape of the F- δ curve; while l and E only affect the amplitude of the F- δ curve without changing its shape, and hence the post-buckling response. Therefore, the type of response (i.e., shape of the F- δ curve) is governed by a relation involving t, h, and ν based on the values of F_n . Thus, the aim here is to determine a critical height-to-thickness ratio, $(h/t)_{cr}$, at which the value of C_n equals zero. This was achieved by examining the effect of ν on C_n (or F_n), see Fig. 14.

From Fig. 14(b) it can be seen that $(h/t)_{cr}$ decreases with an increase in ν . By determining the values of h/t at which $C_n=0$ for several values of ν , a relation between $(h/t)_{cr}$ and ν was obtained as shown in Fig. 16(a). An expression to estimate $(h/t)_{cr}$ was developed in terms of ν and is given in Eq. (13).

$$(h/t)_{cr} = 2.879/\nu^{0.052}. (13)$$

The value of $(h/t)_{cr}$ can be used to design a CCD with a specific stability state. A CCD would have a monostable response if h/t is less than $(h/t)_{cr}$ and a bistable response if h/t is greater than $(h/t)_{cr}$. Fig. 16(b) shows the stability state for the experimentally tested 3D printed specimens with $\nu = 0.33$ and $(h/r)_{cr} = 3.05$ as calculated by Eq.

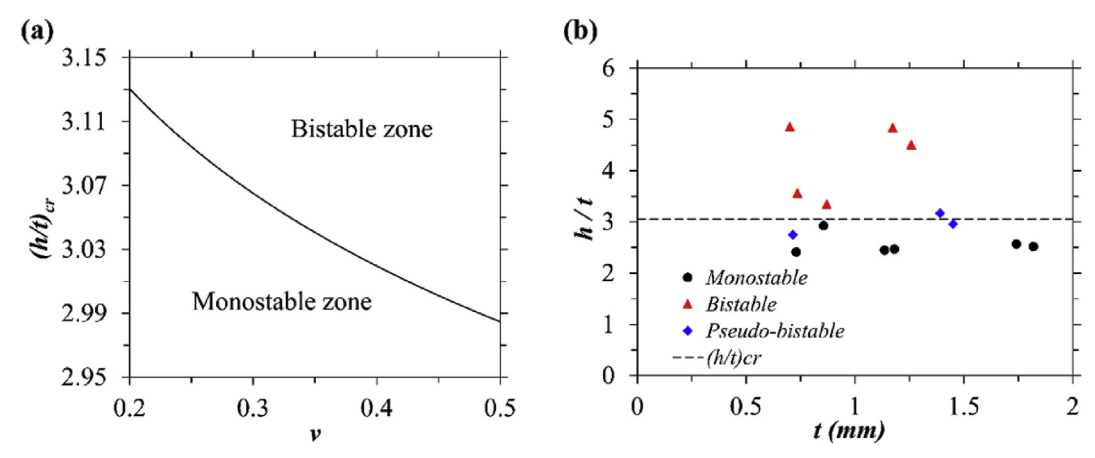


Fig. 16. (a) Critical height-to-thickness ratio $(h/t)_{cr}$ vs. ν ; (b) stability state for 3D printed specimens with $\nu = 0.33$ and $(h/t)_{cr} = 3.05$.

(13). The specimens showed a consistent behavior with the determined limit of $(h/r)_{cr}$. The CCDs below the critical line in Fig. 16(b) had monostable behavior while CCD above the line had bistable behavior. Pseudo-bistable CCDs had h/t close to $(h/r)_{cr}$ and recovered their original configuration after a delay, which indicates viscoelastic material behavior. It should be noted that CCDs with h/t less than 1.5 will exhibit a monotonic $F-\delta$ response and will not have snap-through buckling behavior.

4.7. Example: approximate analysis of single and multiple CCDs

As discussed at the start of Section 4, the multilinear response of a single CCD is useful to obtain the response of a system of multiple CCDs connected in series. The following is an example that illustrates this procedure and compares it to experimental results. It should be noted that a detailed presentation and discussion on the response of multiple CCD is beyond the scope of this work and it is the subject of on-going studies. However, the brief overview provided herein illustrates both the use of CCDs as well as the value of the developed design expressions

Four CCDs were designed and 3D printed with equal nominal dimensions of t=0.6 mm, h=1.8 mm, and l=50 mm. Due to manufacturing imperfections, the 'as printed' dimensions are $t=0.75\pm0.03$ mm, $h=1.76\pm0.02$ mm, and $l=50\pm1$ mm. The material properties are taken as E=817 MPa and $\nu=0.33$. Fig. 17(a) shows the experimental and the FEA $F-\delta$ response of a single CCD. The simplified multilinear response of the CCD specimens, also shown in Fig. 17(a), was constructed using the developed expressions in Eqs. (3) through (12) based on the average dimensions of the printed units. The constructed response slightly underestimates δ_n and F_n ; however, it is in general agreement with the test result. The fabricated specimens recovered their original configuration immediately upon unloading and hence showed a monostable behavior with h/t=2.35, which is smaller than $(h/t)_{CT}$ determined as follows:

$$(h/r)_{cr} = 2.879/\nu^{0.052} = 3.05$$

Four CCDs units with equal nominal dimensions as the single CCD described above were connected in series and the system was tested under displacement control loading as shown in Fig. 18. The resulting F- δ response is shown in Fig. 17(b). The multilinear F- δ response shown in Fig. 17(a) for a single CCD was used to calculate the F- δ response for the four-unit system, as shown in Fig. 17(b). The system response was determined using the model by Benichou and Givli [32]. While the experimental and analytical responses are in relative agreement, the displacement, Δ_{cI} , at the first snap-through event of the experimental response is smaller than that of the multilinear response. This is primarily attributed to dimension variations among the printed CCD units,

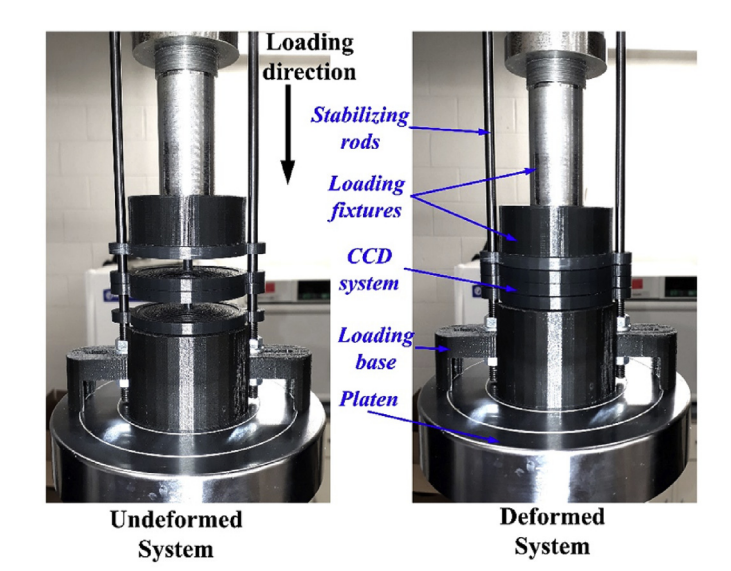


Fig. 18. Test setup for the four CCDs connected in series.

which leads to early snap instability of the CCD with the lowest F_c in the system before the calculated average snap-through displacement $\Delta_{c1}=4\delta_{\rm C}$. In other words, the effective stiffness of the tested system is higher than that based on the calculated average response $(F_c/4\delta_{\rm C})$. Therefore, during loading, the CCD in the system with lowest F_c reaches its limit-point instability $(\delta_{\rm C}, F_c)$ while other CCDs in the system are below their limit.

Although the snap-through limit variation among CCD units complicates calculating an accurate response for the system, it is an essential feature to obtain a response with progressive snapping instabilities, and hence elastic energy dissipation. The area enclosed between the experimental loading and unloading curves represent the elastic strain energy dissipated by the system. This area depends on the number of connected units and h/t.

5. Conclusions

The presented study showed that cosine-curved domes (CCDs) with constrained edges loaded under a concentrated apex transverse load can attain snap-through instability with symmetric deformations, even with some imperfections. This was validated through finite element simulations and testing of 3D printed specimens for CCDs within the geometrical range of $1.5 \le h/t \le 7.5$ and $h/l \le 1/16$. However, CCDs with higher h/t and h/l ratios are more susceptible to bifurcation and asymmetric deformations. In addition, CCDs within the noted geometry

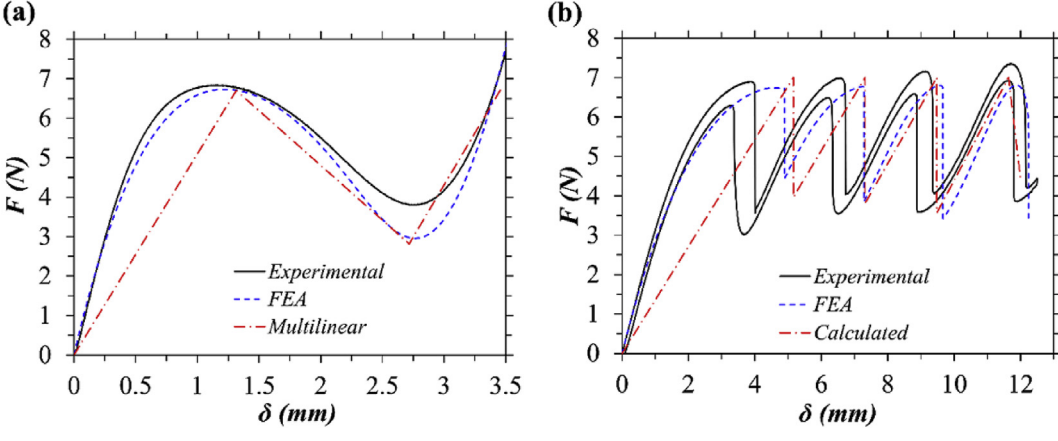


Fig. 17. Experimental, FEA, and approximate multilinear F- δ responses of (a) a single CCD, and (b) system of 4 CCDs connected in series.

range do not require the restriction of other buckling modes to have a symmetric reversible snapping, offering a multistable element that could be used as a building unit for devices subjected to relatively high forces for energy dissipation and repeated use.

Three types of snap-through instability responses were recognized for the studied CCDs: monostable, pseudo-bistable, and bistable responses. The main factor affecting the response is the height-to-thickness ratio (h/t). Increase of h/t changes the response from monostable to bistable. Increasing value of the material's Poisson's ratio (ν) decreases the value of the minimum force (F_n) , which could change the instability type from monostable to bistable. The study also showed that the base diameter (1) affects the values of the force-deformation curve but it has no effect on its shape. It was found that CCDs have a critical height-to-thickness ratio $(h/t)_{cr}$ at which the response is pseudo-bistable $(F_n = 0)$. This allows designing CCDs with a targeted snap-through instability type. The ratio is independent of the geometric and material properties except for ν . However, the effect of ν on $(h/t)_{cr}$ is small for common materials. $(h/t)_{cr}$ may be taken as a constant value of 3.045. Expressions to estimate key parameters in the force-deformation response were developed to construct a multilinear force-deformation response, and shown to facilitate the response analysis for a system of multiple CCDs.

The multistable elastic behavior possessed by CCDs originates from the cosine curved profile that allows them to have a tunable multistable response. The proposed CCDs offer controllable elastic snap-through behavior that could be used as a building block for elastic energy dissipation mechanisms subjected to relatively high forces. Future studies on the response of CCDs should include the influence of manufacturing imperfections and loading direction.

References

- M. Radwanska, A. Stankiewicz, A. Wosatko, J. Pamin, Plate and Shell Structures, (2017), https://doi.org/10.1002/9781118934531.
- B. Fedelich, G. Zanzotto, Hysteresis in discrete systems of possibly interacting elements with a double-well energy, J. Nonlinear Sci. 2 (1992) 319–342, https://doi.org/10.1007/BF01208928.
- [3] Z.P. Bažant, L. Cedolin, Stability of Structures: Elastic, Inelastic, Fracture and Damage Theories, World Scientific, 2010, https://doi.org/10.1142/7828.
- [4] D.M. Correa, T. Klatt, S. Cortes, M. Haberman, D. Kovar, C. Seepersad, Negative stiffness honeycombs for recoverable shock isolation, Rapid Prototyp. J. 21 (2015) 193–200, https://doi.org/10.1108/RPJ-12-2014-0182.
- [5] S. Shan, S.H. Kang, J.R. Raney, P. Wang, L. Fang, F. Candido, J.A. Lewis, K. Bertoldi, Multistable Architected materials for trapping elastic strain energy, Adv. Mater. 27 (2015) 4296–4301, https://doi.org/10.1002/adma.201501708.
- [6] A. Rafsanjani, A. Akbarzadeh, D. Pasini, Snapping mechanical metamaterials under tension, Adv. Mater. 27 (2015) 5931–5935, https://doi.org/10.1002/adma. 201502809.
- [7] T. Frenzel, C. Findeisen, M. Kadic, P. Gumbsch, M. Wegener, Tailored buckling microlattices as reusable light-weight shock absorbers, Adv. Mater. 28 (2016) 5865–5870, https://doi.org/10.1002/adma.201600610.
- [8] N. Kidambi, R.L. Harne, K.W. Wang, Energy capture and storage in asymmetrically multistable modular structures inspired by skeletal muscle, Smart Mater. Struct. 26 (2017) 1–15, https://doi.org/10.1088/1361-665X/aa721a.
- [9] C.S. Ha, R.S. Lakes, M.E. Plesha, Design, fabrication, and analysis of lattice exhibiting energy absorption via snap-through behavior, Mater. Des. 141 (2018)

- 426-437, https://doi.org/10.1016/j.matdes.2017.12.050.
- [10] J. Qiu, J.H. Lang, A.H. Slocum, A curved-beam bistable mechanism, J. Microelectromech. Syst. 13 (2004) 137–146, https://doi.org/10.1109/JMEMS. 2004.825308.
- [11] N. Lajnef, R. Burgueño, W. Borchani, Y. Sun, A concept for energy harvesting from quasi-static structural deformations through axially loaded bilaterally constrained columns with multiple bifurcation points, Smart Mater. Struct. 23 (2014), https:// doi.org/10.1088/0964-1726/23/5/055005.
- [12] S. Liu, R. Burgueño, Controlled elastic postbuckling of bilaterally constrained non-prismatic columns: application to enhanced quasi-static energy harvesters, Smart Mater. Struct. 25 (2016), https://doi.org/10.1088/0964-1726/25/12/125010.
- [13] P. Cazottes, A. Fernandes, J. Pouget, M. Hafez, Bistable buckled beam: modeling of actuating force and experimental validations, J. Mech. Des. 131 (2009) 101001–101010 https://doi.org/10.1115/1.3179003.
- [14] R. Burgueño, N. Hu, A. Heeringa, N. Lajnef, Tailoring the elastic postbuckling response of thin-walled cylindrical composite shells under axial compression, Thin-Walled Struct. 84 (2014) 14–25, https://doi.org/10.1016/j.tws.2014.05.009.
- [15] N. Hu, R. Burgueño, Elastic postbuckling response of axially-loaded cylindrical shells with seeded geometric imperfection design, Thin-Walled Struct. 96 (2015) 256–268, https://doi.org/10.1016/j.tws.2015.08.014.
- [16] S. Palathingal, G.K. Ananthasuresh, Design of bistable arches by determining critical points in the force-displacement characteristic, Mech. Mach. Theor. 117 (2017) 175–188 https://doi.org/10.1016/j.mechmachtheory.2017.07.009.
- [17] L.N. Virgin, Y. Guan, R.H. Plaut, On the geometric conditions for multiple stable equilibria in clamped arches, Int. J. Non-Linear Mech. 92 (2017) 8–14.
- [18] Y. Guan, L.N. Virgin, D. Helm, Structural behavior of shallow geodesic lattice domes, Int. J. Solids Struct. 155 (2018) 225–239.
- [19] D. Orlando, C. Henrique, P.B. Gonçalves, Nonlinear vibrations and instability of a bistable shallow reticulated truss, Nonlinear Dynam. 94 (2018) 1479–1499, https://doi.org/10.1007/s11071-018-4437-1.
- [20] J.F. Mescall, Large deflections of spherical shells under concentrated loads, J. Appl. Mech. 32 (1965) 936, https://doi.org/10.1115/1.3627340.
- [21] F.A. Penning, Experimental buckling modes of clamped shallow shells under concentrated load, J. Appl. Mech. (1966), https://doi.org/10.1115/1.3625041.
- [22] J.R. Fitch, The buckling and post-buckling behavior of spherical caps under concentrated load, Int. J. Solids Struct. 4 (1968) 421–446, https://doi.org/10.1016/0020-7683(68)90048-6.
- [23] G.W. Brodland, H. Cohen, Deflection and snapping of spherical caps, Int. J. Solids Struct. 23 (1987) 1341–1356, https://doi.org/10.1016/0020-7683(87)90001-1.
- [24] A. Brinkmeyer, M. Santer, A. Pirrera, P.M. Weaver, Pseudo-bistable self-actuated domes for morphing applications, Int. J. Solids Struct. 49 (2012) 1077–1087, https://doi.org/10.1016/j.ijsolstr.2012.01.007.
- [25] A. Madhukar, D. Perlitz, M. Grigola, D. Gai, K. Jimmy Hsia, Bistable characteristics of thick-walled axisymmetric domes, Int. J. Solids Struct. 51 (2014) 2590–2597, https://doi.org/10.1016/j.ijsolstr.2014.03.022.
- [26] M. Vangbo, An analytical analysis of a compressed bistable buckled beam, Sensor Actuator A Phys. 69 (1998) 212–216 https://doi.org/10.1016/S0924-4247(98) 00007-1
- [27] Dassault Systèmes, Abaqus User Manual, (2012).
- [28] C.S. Lee, S.G. Kim, H.J. Kim, S.H. Ahn, Measurement of anisotropic compressive strength of rapid prototyping parts, J. Mater. Process. Technol. 187–188 (2007) 627–630, https://doi.org/10.1016/j.jmatprotec.2006.11.095.
- [29] C. Casavola, A. Cazzato, V. Moramarco, C. Pappalettere, Orthotropic mechanical properties of fused deposition modelling parts described by classical laminate theory, Mater. Des. 90 (2016) 453–458, https://doi.org/10.1016/j.matdes.2015. 11.009.
- [30] C. Perkowski, Tensile-compressive Asymmetry and Anisotropy of Fused Deposition Modeling PLA under Monotonic Conditions, University of Central Florida, 2017, http://stars.library.ucf.edu/etd/5576.
- [31] Scott A. Pardo, Empirical Modeling and Data Analysis for Engineers and Applied Scientists, (2016), https://doi.org/10.1007/978-3-319-32768-6 Springe, NJ.
- [32] I. Benichou, S. Givli, Structures undergoing discrete phase transformation, J. Mech. Phys. Solids 61 (2013) 94–113 https://doi.org/10.1016/j.jmps.2012.08.009.
- [33] D. Restrepo, N.D. Mankame, P.D. Zavattieri, Phase transforming cellular materials, Extrem. Mech. Lett. 4 (2015) 52–60, https://doi.org/10.1016/j.eml.2015.08.001.